JOURNAL OF SCIENCE TECHNOLOGY AND EDUCATION 14(3), SEPTEMBER, 2026
E-ISSN: 3093-0898, PRINT ISSN: 2277-0011; Journal homepage: www.atbufstejoste.com

Thermal Simulation and Experimental Validation of a 1.5 kW Three-Phase Squirrel-Cage Induction Motor using Finite Element Analysis

[1]Onwe Peter Daffin, [2]Okoro Ogbonnaya Inya, [3]Patrick Otubu Odu
[1&3]Department of Electrical and Electronic Engineering, University of Calabar, Nigeria
[2]Department of Electrical and Electronic Engineering, Micheal Okpara University of Agriculture

ABSTRACT

This study investigates the thermal behaviour of a 1.5 kW, three-phase squirrel-cage induction motor operating at rated load. The motor was modelled in ANSYS Motor-CAD using its geometry, winding arrangement, material properties, and rated operating conditions. The thermal model was used to determine the temperatures of different parts of the motor during operation. MATLAB was used to process and present the simulation results. The temperatures considered were those of the housing, stator back iron, rotor back iron, rotor bars, and stator winding. Temperature measurements were also taken from the physical motor at a supply voltage of 380 V and compared with the simulated results. The measured ambient, housing, stator back-iron, and rotor back-iron temperatures were 30.05°C, 52.2°C, 55.1°C, and 59.2°C, respectively. The corresponding simulated temperatures were 30.05°C, 47.29°C, 62.38°C, and 51.51°C. The percentage differences were 0%, 9.41%, 13.21%, and 12.99%, respectively. The simulation also gave an average rotor-bar temperature of 51.67°C and a winding temperature of 80.54°C. No experimental measurements were available for the rotor bars and winding. The results show that the thermal model gives a reasonable estimate of the temperature distribution of the motor at rated load, although some differences were observed between the measured and simulated temperatures.

ARTICLE INFO
Article History
Received: April, 2026
Received in revised form: May, 2026
Accepted: August, 2026
Published online: September, 2026

KEYWORDS
Squirrel-Cage Induction Motor; Thermal Analysis; Motor-CAD; Rated Load; Temperature Distribution; Thermal Modelling; Experimental Validation.

INTRODUCTION

Three-phase squirrel-cage induction motors are widely used in industrial applications because of their simple construction, reliability, and relatively low maintenance requirements [1], [8], [10]. They are commonly used in equipment such as pumps, fans, compressors, conveyors, and machine tools. Temperature is an important factor in the operation of an induction motor. During operation, heat is produced in different parts of the motor as a result of electrical and mechanical losses. Stator copper loss, rotor losses, core loss, friction, and windage all contribute to the heat generated inside the machine. If the temperature becomes too high, particularly in the winding, the insulation can deteriorate and the service life of the motor can be reduced. For this reason, thermal analysis is important when assessing the operating condition of an induction motor. Several methods have been used to predict motor temperature. Lumped parameter thermal networks have been applied to estimate the temperature of different motor components [3], [7], while combined electromagnetic and thermal models have also been used to study the heat distribution in induction machines [9], [10].

Okoro [1] investigated the steady-state and transient thermal behaviour of a squirrel-cage induction motor operating at rated load. Afrah and Amer [2] used Motor-CAD, Flux2D, and MATLAB for the thermal analysis of a three-phase induction motor. Other researchers have investigated thermal modelling, thermal stresses, and the effects of motor operating conditions on temperature [3], [6], [11]–[13].

Corresponding author: Onwe Peter Daffin
peteronwe@unical.edu.ng
Department of Electrical and Electronic Engineering, University of Calabar, Nigeria.

JOURNAL OF SCIENCE TECHNOLOGY AND EDUCATION 14(3), SEPTEMBER, 2026
E-ISSN: 3093-0898, PRINT ISSN: 2277-0011; Journal homepage: www.atbufstejoste.com

Although simulation can provide temperature information for different parts of a motor, measurements from an actual machine are useful for checking the accuracy of the thermal model. Differences between measured and simulated temperatures may result from assumptions concerning material properties, heat-transfer conditions, losses, cooling, and the physical construction of the motor.

This study therefore examines the thermal behaviour of a 1.5 kW three-phase squirrel-cage induction motor at rated load using ANSYS Motor-CAD. The temperatures of the housing, stator back iron, rotor back iron, rotor bars, and stator winding were obtained from the simulation. Measurements were also taken from the physical motor at a supply voltage of 380 V and compared with the simulated results.

The aim of the study is to determine how closely the simulated temperatures agree with measurements obtained from the actual motor under rated-load operation.

Thermal and Electromagnetic Loss Model

The temperature developed in an induction motor depends largely on the heat produced by its electrical and mechanical losses. The main sources of heat considered in the thermal analysis are stator copper loss, core loss, rotor loss, friction, and windage.

The thermal behaviour of the motor can be described using the heat-conduction equation:

$$\rho c \frac{\partial T}{\partial t} = \nabla \cdot (k \nabla T) + Q \qquad 1$$

Where ρ is the material density (kg/m³), c is the specific heat capacity (J/kg·K), T is the temperature (°C or K), t is time(s), k is thermal conductivity (W/m·K), ∇ is the vector differential (gradient/divergence) operator, Q is the volumetric heat generation rate (W/m³). The heat generated inside the motor is related to its losses. In this study, the total heat generation was considered from the major motor losses:

The motor was modelled using a lumped parameter thermal network (LPTN), in which thermal resistances are given by

$$P_{loss} = P_{cu} + P_{iron} + P_{mech} + P_{other} \qquad 2$$

Where P_{cu} is the copper loss, P_{iron} is the core loss, P_{mech} represents mechanical losses, and P_{other} represents other losses included in the model.

The stator copper losses calculated as

$$P_{cu} = 3I^2 R_T \qquad 3$$

Where; P_{cu} is three-phase stator copper loss (W),I is the phase current and R_T is the winding resistance at the operating temperature. Since copper resistance changes with temperature, the winding resistance can be represented by

$$R_T = R_0[1 + \alpha(T - T_0)] \qquad 4$$

Where R_0 is the stator winding resistance at the reference temperature T_0(Ω), α is the temperature coefficient of resistance for copper (°C^{-1}), T is the operating winding temperature (°C), T_0 is the reference temperature (°C)

Motor Specification

The motor used in the study is a 1.5 kW, three-phase squirrel-cage induction motor. The main parameters used in the Motor-CAD model are presented in Table 1

Table 1: Motor specification and geometry

Parameters	Value
Rated power	1.5 kW
Rated voltage	380 V
Rated current	3.83 A
Rated speed	1430 rpm
Frequency	50 Hz
Pole number	4
Slot number	24
Stator lamination diameter	170mm
Stator bore	98.6mm
Tooth width	10mm
Rotor bars	34
Slot depth	25mm
Yoke thickness	12mm
Airgap	1mm
Shaft diameter	28mm
Rotor diameter	96.6mm
Rotor tooth width	4mm
Bar opening	1.5mm
Bar depth	10mm

Corresponding author: Onwe Peter Daffin
peteronwe@unical.edu.ng
Department of Electrical and Electronic Engineering, University of Calabar, Nigeria.

The motor has four poles and operates from a 50 Hz supply. Its synchronous speed is therefore 1500 rpm, while the specified rated speed is 1430 rpm. The difference between these speeds is expected in an induction motor because rotor slip is required for the induction of rotor current and the production of torque. The motor geometry was entered in Motor-CAD using the dimensions listed in Table 1. The stator contains 24 slots and the rotor has 34 bars. The air gap was set to 1 mm and the shaft diameter was set to 28 mm. These dimensions determine the active electromagnetic regions as well as the thermal paths used in the model.

The winding arrangement and the material assigned to each region were also defined before the thermal calculation. The stator, rotor, shaft, winding and housing were treated as separate parts so that the temperature of each region could be obtained after the simulation. The rated voltage of 380 V and frequency of 50 Hz were used for the operating condition. The rated-load condition was selected because it represents the normal design operating point of the motor. Thermal studies at rated load are also relevant to the assessment of temperature rise and continuous operation [1], [7].

Thermal Model

The motor was modelled in ANSYS Motor-CAD using the specified geometry, winding arrangement, material properties, and rated operating conditions. The thermal model considers heat generated within the motor and the movement of heat from the internal components to the housing and surrounding air. The thermal calculation was based on the heat generated by the electromagnetic and mechanical losses. These losses were assigned to the appropriate motor regions. The model then calculated the temperature of the housing, stator back iron, rotor back iron, rotor bars and winding.

The main steps used in the thermal modelling were:

1. development of the motor geometry;
2. assignment of material properties to the motor regions;
3. definition of the winding and rotor cage;
4. setting of the rated voltage, frequency and load;
5. calculation of the electromagnetic losses;
6. transfer of the calculated losses to the thermal model; and
7. calculation and extraction of the temperature distribution.

The thermal analysis was carried out for both transient and steady-state operation. The transient calculation was used to observe the rise in temperature with time, while the steady-state calculation was used to obtain the final temperatures after the motor had operated long enough for the thermal response to settle.

A lumped parameter thermal network was used to represent the main heat-transfer paths in the motor. The thermal resistance of a heat-transfer path can be expressed as:

$$R_{th} = \frac{L}{kA} \qquad 5$$

Where R_{th} is the thermal resistance (K/W), L is the heat conduction path length (m), k is the thermal conductivity of the material (W/m·K), A is the cross-sectional area normal to heat flow (m²)
The model was used to determine the temperatures of the housing, stator back iron, rotor back iron, rotor bars, and stator winding.

The finite element model was developed from the motor geometry and material properties, and the thermal calculation was performed under the rated-load operating condition. The modelling process involved defining the motor geometry, assigning the material properties, specifying the winding and operating conditions, generating the computational model, and calculating the temperature distribution.

Electromagnetic Losses for the Thermal Model

The thermal behaviour of the motor depends on the losses produced during operation. In this study, ANSYS Motor-CAD was used to calculate the electromagnetic losses from the motor geometry, winding arrangement, material properties, supply conditions, and rated-load operation. These losses were then used as heat

Corresponding author: Onwe Peter Daffin
peteronwe@unical.edu.ng
Department of Electrical and Electronic Engineering, University of Calabar, Nigeria.

JOURNAL OF SCIENCE TECHNOLOGY AND EDUCATION 14(3), SEPTEMBER, 2026
E-ISSN: 3093-0898, PRINT ISSN: 2277-0011; Journal homepage: www.atbufstejoste.com

sources in the thermal model as presented in figure 1 and table 2

The main losses considered in the thermal analysis were stator copper loss, rotor losses, iron loss, and mechanical losses. The losses generated inside the motor increase the temperature of the different components, while heat is transferred from the internal parts to the motor housing and then to the surrounding air. The electromagnetic and thermal calculations were linked in Motor-CAD so that the losses obtained from the motor operating condition could be used to determine the temperature distribution. The thermal analysis was carried out for the stator winding, stator back iron, rotor back iron, rotor bars, and housing.

The modelling procedure involved:

1. defining the motor geometry;
2. assigning the material properties;
3. defining the stator winding and rotor cage;
4. setting the rated voltage, frequency, and load;
5. calculating the electromagnetic losses;
6. applying the losses to the thermal model; and
7. obtaining the temperature distribution of the motor components.

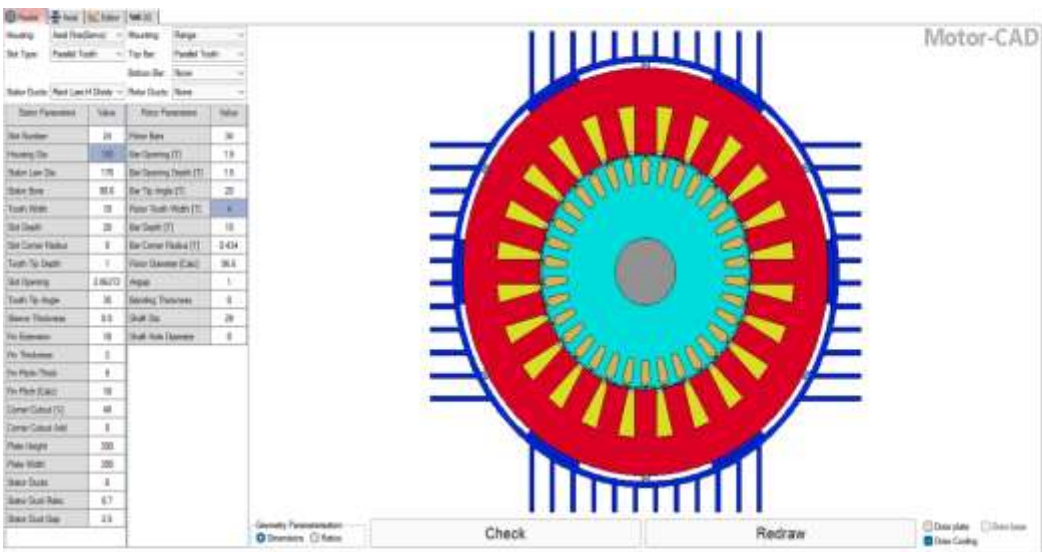

Figure 1; Radial temperature distribution of the studied induction motor

Material Properties

The material properties used in Motor-CAD were assigned according to the materials selected for the stator, rotor, winding, shaft and other motor regions. Thermal conductivity, density and specific heat are important because they affect how quickly heat moves through each component and how much heat the material can store. Electrical and magnetic properties also affect the calculated losses that serve as heat sources.

Corresponding author: Onwe Peter Daffin
peteronwe@unical.edu.ng
Department of Electrical and Electronic Engineering, University of Calabar, Nigeria.

JOURNAL OF SCIENCE TECHNOLOGY AND EDUCATION 14(3), SEPTEMBER, 2026
E-ISSN: 3093-0898, PRINT ISSN: 2277-0011; Journal homepage: www.atbufstejoste.com

Table 2: Material properties of the motor

Component	Material from Database	Electrical Resistivity	Temp Coef Electrical Resistivity	Magnet Br at 20°C	Magnet Relative Permeability	Temp Coef Br	Density	Weight	Notes
Units		Ohm.m		Tesla			kg/m³	kg	
Stator Lam (Back Iron)	M350-50A	4.4E-07	0				7650	5.083	
Stator Lam (Tooth)	M350-50A	4.4E-07	0				7650	3.212	
Stator Lamination [Total]								8.295	
Armature Winding [Active]	Copper (Annealed)	1.724E-08	0.00393				8933	0.8278	
Armature EWdg [Front]	Copper (Annealed)	1.724E-08	0.00393				8933	0.7239	
Armature EWdg [Rear]	Copper (Annealed)	1.724E-08	0.00393				8933	0.7239	
Armature Winding [Total]								2.276	
Slot Wedge							1000	0.0007295	
Rotor Lam (Back Iron)	M350-50A	4.4E-07	0				7650	2.43	
Rotor Lam (Tooth)	M350-50A	4.4E-07	0				7650	1.177	
Rotor Lamination [Total]								3.607	
Rotor Cage Top Bar	Copper (Pure)	1.724E-08	0.003862				8933	0.993	
Rotor Cage Top Bar Opening	Copper (Pure)	1.724E-08	0.003862				8933	0.06166	
Rotor Cage (Front End)	Aluminium (Cast)	3.3E-08	0.00375				2950	0.1225	
Rotor Cage (Rear End)	Aluminium (Cast)	3.3E-08	0.00375				2950	0.1225	
Rotor Cage [Total]								1.3	
Stator Bore Sleeve							4000	0.1294	
Shaft [Active]							7800	0.4323	
Shaft [Front]							7800	0.3637	
Shaft [Rear]							7800	0.2489	
Shaft [Total]								1.045	
Total Weight								16.65	Weight [Total]

Experimental Method

Temperature measurements were taken from the physical three-phase induction motor and compared with the Motor-CAD results. The test setup consisted of a three-phase power supply, three-phase variac, protection and distribution unit, measuring instruments, induction motor, loading machine, tachometer, and infrared thermometer.

An oscilloscope was used to check the supply voltage waveform. The motor speed was measured with an infrared tachometer, while an infrared thermometer was used to measure the temperature of the accessible parts of the motor. The motor was operated at 380 V, which is the rated supply voltage. Temperature measurements were taken from the ambient environment, housing, stator back iron, and rotor back iron.

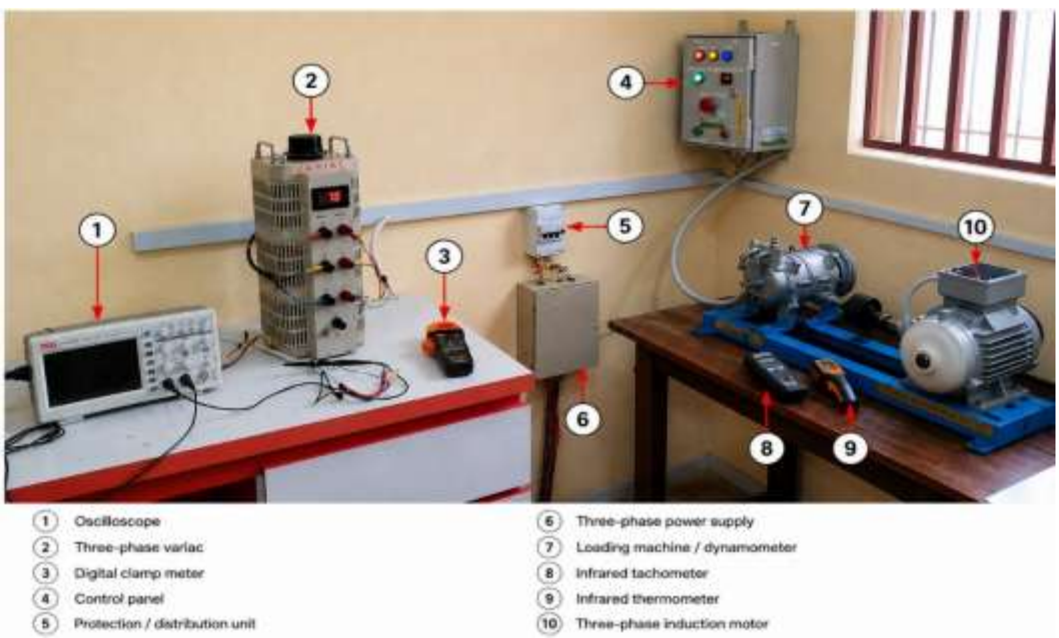

Plate1: Experimental setup

Corresponding author: Onwe Peter Daffin
peteronwe@unical.edu.ng
Department of Electrical and Electronic Engineering, University of Calabar, Nigeria.

JOURNAL OF SCIENCE TECHNOLOGY AND EDUCATION 14(3), SEPTEMBER, 2026
E-ISSN: 3093-0898, PRINT ISSN: 2277-0011; Journal homepage: www.atbufstejoste.com

The experimental measurements are presented in table 3:

Table 3: Experimental measurement of the motor at rated load

S/No	Temperature	Values	Unit
1	Ambient	30	°C
2	Housing	52.2	°C
3	Stator back iron	55.1	°C
4	Rotor back iron	56.2	°C

These measurements were used directly for comparison with the corresponding Motor-CAD results.

Steady-State Thermal Simulation Results

The principal steady-state simulation results obtained from Motor-CAD are presented in Table 4. The ambient temperature in the simulation was 30.05°C, which is almost the same as the measured ambient temperature. This provides a suitable basis for comparing the other temperatures. The simulated housing temperature was 47.29°C. It was lower than the temperatures of the stator back iron and winding. This is expected because heat generated inside the motor must pass through the internal parts before reaching the housing and being released to the surrounding air.

The stator back iron reached 62.38°C. This was higher than the simulated rotor back iron temperature of 51.51°C. Heat generated in the stator winding contributes to the temperature of the stator core, which helps explain the higher temperature obtained in this region. The average rotor-bar temperature was 51.67°C, which was close to the rotor back-iron temperature of 51.51°C. This indicates that the two rotor regions had similar temperatures in the simulation. The highest temperature was obtained in the stator winding at 80.54°C. This is important because the winding is directly affected by the copper losses produced by the current flowing through the conductors.

Table 4: Steady-state simulation results at rated load

S/No	Description of temperature	Values	Units
1	Ambient	30.05	°C
2	Housing	47.29	°C
3	Stator back iron	62.38	°C
4	**Rotor back iron**	51.51	°C
5	Rotor bar average	51.67	°C
6	Winding	80.54	°C

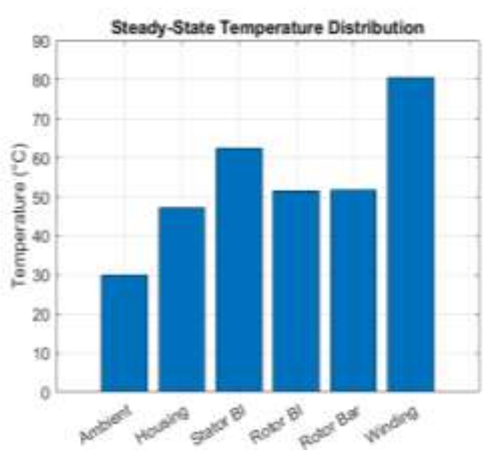

Figure 4: steady-state temperature distribution

Transient Thermal Results

The transient simulation was used to observe how the motor temperature changes with operating time at rated load. The temperature does not reach its final value immediately after the motor is started. Instead, heat builds up as the motor continues to operate. At the beginning of operation, the temperature is close to the ambient condition. As the motor runs, electrical and mechanical losses generate heat within the motor. The temperature therefore increases with time.

As operation continues, the difference between the motor temperature and the surrounding temperature increases. This causes more heat to leave the motor through conduction,

Corresponding author: Onwe Peter Daffin
peteronwe@unical.edu.ng
Department of Electrical and Electronic Engineering, University of Calabar, Nigeria.

convection, and other cooling paths. The rate of temperature rise therefore becomes smaller until the motor approaches a steady thermal condition. The transient temperature distribution obtained from the simulation is presented in figure 4

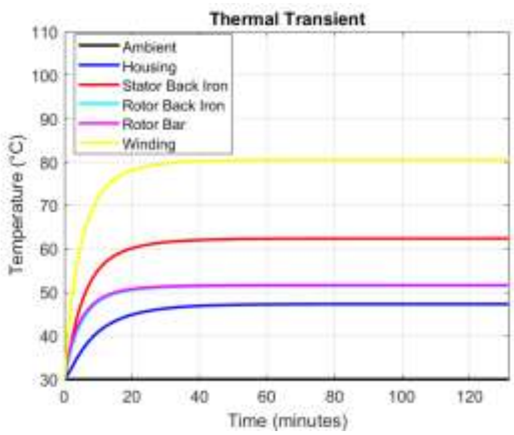

Figure 5: Transient-state temperature distribution at rated load

Experimental Validation

The simulated and measured temperatures are compared in Table 5. The ambient temperature showed almost exact agreement between the experiment and simulation. The measured value was 30.05°C, while the simulated value was 30.00°C. For the housing, the measured temperature was 52.2°C compared with 47.29°C from the simulation. The difference was 9.41%. The simulation therefore gave a lower housing temperature than the experiment.

The measured stator back-iron temperature was 55.1°C, while the simulation gave 62.38°C. The difference was 13.21%. In this case, the simulation predicted a higher temperature than the measurement. For the rotor back iron, the measured temperature was 59.2°C, while the simulated temperature was 51.51°C. The difference was 12.99%. No experimental measurements were recorded for the rotor bars or the stator winding. Therefore, the simulated values of 51.67°C and 80.54°C for these two components cannot be directly validated using the present experimental data.

Table 5: steady-state comparison of experimental and simulated results at rated load

S/No	Parameters	Experimental results	Simulated results	Percentage Difference
1	Ambient	30.05 °C	30.00 °C	0 %
2	Housing	52.2 °C	47.29 °C	9.41 %
3	Stator back iron	55.1 °C	62.38 °C	13.21 %
4	Rotor back iron	59.2 °C	51.51 °C	12.99 %
5	Rotor bar average	Nil	51.67 °C	Nil
6	Winding	Nil	80.54 °C	Nil

DISCUSSION OF FINDINGS

The results show that the motor has a clear temperature difference between its internal components and the housing. The winding recorded the highest simulated temperature at 80.54°C. The stator back iron was 62.38°C, while the rotor back iron and rotor-bar average temperatures were 51.51°C and 51.67°C. The housing was the coolest of the listed motor components at 47.29°C. The high winding temperature is consistent with the fact that the winding is one of the main locations where electrical loss is produced. The heat generated in the conductors is transferred to the stator core and then towards the housing. This explains why the stator back iron is also warmer than the housing. Similar relationships between motor losses and component temperatures have been reported in previous thermal studies [1], [7], [9], [10].

The simulated stator back-iron temperature was higher than the rotor back-iron temperature. The experimental result, however, showed the rotor back iron at 59.2°C and the stator back iron at 55.1°C. This difference between the simulation and experiment suggests that the actual heat-transfer paths in the physical motor differ to some extent from those represented in the model.

Corresponding author: Onwe Peter Daffin
peteronwe@unical.edu.ng
Department of Electrical and Electronic Engineering, University of Calabar, Nigeria.

The housing difference of 9.41% is lower than the differences obtained for the stator and rotor back iron. The housing is directly exposed to the surrounding air, so its temperature is influenced by ambient conditions, ventilation, surface condition, motor position and the heat-transfer coefficient used in the model. These factors can change the measured housing temperature even when the internal losses remain the same [11].

The 13.21% difference obtained for the stator back iron was the largest among the measured stator and rotor components. The simulation gave 62.38°C compared with 55.1°C measured experimentally. The result may be affected by the assumed material properties, heat-transfer coefficients, loss distribution and exact location of the infrared measurement. The rotor back iron showed a difference of 12.99%, with the simulation giving a lower temperature than the measured value. Rotor temperature prediction can be particularly sensitive to the way rotor losses and heat-transfer paths are represented. Ahmed and Kar [9] also showed that the thermal behaviour of the rotor and end-winding regions can be affected by the details of the thermal model.

The winding temperature of 80.54°C is important even though it was not experimentally measured. The winding is usually one of the most thermally sensitive parts of an induction motor because of the electrical loss generated in its conductors. A direct measurement of the winding temperature would therefore be useful in a future validation test.

The results also show why experimental validation should be performed at the same operating condition used in the simulation. The present comparison was made at the rated 380 V supply. Using the same voltage and rated-load condition reduces one source of variation between the numerical and experimental results. The thermal model is useful for estimating internal temperatures that cannot be measured easily. In particular, the simulated winding temperature and rotor-bar temperature provide information that was not available from the experimental measurements. However, these values should be treated as model predictions rather than experimentally validated temperatures.

The study agrees with earlier work in showing that thermal modelling can be used to estimate the temperature behaviour of induction machines [1]–[3], [7], [10], [11]. The present work adds an experimental comparison for a 1.5 kW motor operating at rated load. This is useful because the accuracy of a thermal model depends not only on the mathematical formulation but also on the actual construction and cooling conditions of the machine.

Some limitations should be recognised. First, only a limited number of motor locations could be measured experimentally. The winding and rotor-bar temperatures were not directly available. Second, an infrared thermometer measures surface temperature and may be affected by surface emissivity and the exact position of the measurement. Third, the thermal model depends on the material and cooling parameters entered in Motor-CAD. Improving these inputs may reduce the differences between the simulation and experiment.

For further work, temperature sensors could be installed at selected internal or accessible locations to obtain additional measurements. The thermal model could also be refined using measured heat-transfer conditions and more accurate material data. These improvements would provide a stronger comparison between the calculated internal temperatures and the actual motor temperatures. Despite these limitations, the present results provide a useful picture of the rated-load thermal condition of the motor. The simulated winding temperature identifies the winding as the hottest component, while the comparison of the housing, stator back iron and rotor back iron gives a practical check on the model.

CONCLUSION

A thermal model of a 1.5 kW three-phase squirrel-cage induction motor was developed in ANSYS Motor-CAD and used to study the temperature distribution of the motor at rated load. The simulation considered the

Corresponding author: Onwe Peter Daffin
peteronwe@unical.edu.ng
Department of Electrical and Electronic Engineering, University of Calabar, Nigeria.

JOURNAL OF SCIENCE TECHNOLOGY AND EDUCATION 14(3), SEPTEMBER, 2026
E-ISSN: 3093-0898, PRINT ISSN: 2277-0011; Journal homepage: www.atbufstejoste.com

housing, stator back iron, rotor back iron, rotor bars, and stator winding.

The highest simulated temperature was obtained in the winding at 80.54°C, followed by the stator back iron at 62.38°C. The rotor back iron and rotor bars reached 51.51°C and 51.67°C, respectively, while the housing temperature was 47.29°C. Experimental measurements were taken at a supply voltage of 380 V. The measured temperatures of the ambient, housing, stator back iron, and rotor back iron were 30.05°C, 52.2°C, 55.1°C, and 59.2°C, respectively. The corresponding simulated values were 30.00°C, 47.29°C, 62.38°C, and 51.51°C. The percentage differences were 0%, 9.41%, 13.21%, and 12.99%, respectively.

The differences between the measured and simulated temperatures show that the thermal model gives a reasonable representation of the motor under rated-load operation. However, the results also show that the heat-transfer conditions and other thermal parameters in the model could be improved. Direct measurements of the winding and rotor-bar temperatures would also provide a better basis for validating the internal temperature predictions.

REFERENCES

1. O. I. Okoro, "Steady and transient states thermal analysis of a 7.5-kW squirrel-cage induction machine at rated-load operation," *IEEE Transactions on Energy Conversion*, vol. 20, no. 4, pp. 730–735, 2005.
2. T. A. Afrah and A. M. Amer, "Thermal analysis of a three-phase induction motor based on Motor-CAD, Flux2D and MATLAB," *Indonesian Journal of Electrical Engineering and Computer Science*, vol. 15, no. 1, pp. 46–53, 2019.
3. S. E. Oti, J. Ugwu, D. B. Nnadi, and U. Ogbuefi, "Development and thermal modeling of an induction machine," *International Journal of Engineering & Technology*, vol. 8, no. 4, pp. 500–508, 2019.
4. E. J. Akpama, O. I. Okoro, and E. Chikuni, "Simulation of the performance of induction machine under unbalanced source voltage conditions," *Pacific Journal of Science and Technology*, vol. 11, no. 1, pp. 9–15, 2010.
5. E. J. Akpama, I. E. Omini, E. E. Effiong, and R. U. Ezenwosu, "PID speed-controlled model of induction motor using Simulink," *International Journal of Engineering Research and Management*, vol. 7, no. 10, pp. 24–28, 2020.
6. O. S. Ejiofor, J. Ugwu, N. D. Benneth, and U. Ogbuefi, "Development and thermal modeling of an induction machine," *International Journal of Engineering & Technology*, vol. 8, no. 4, pp. 500–508, 2019.
7. O. S. Ejiofor, C. Awah, C. Nnonyelu, and O. I. Okoro, "Thermal modelling and analysis of a 10HP induction machine using the lumped parameter approach," *International Journal of Integrated Engineering*, vol. 13, no. 6, 2021.
8. E. C. Abunike, O. I. Okoro, and G. D. Umoh, "Steady and dynamic states analysis of induction motor: FEA approach," *Nigerian Journal of Technology*, vol. 36, no. 4, pp. 1202–1207, 2017.
9. F. Ahmed and N. C. Kar, "Analysis of end-winding thermal effects in a totally enclosed fan-cooled induction motor with die-cast copper rotor," *IEEE Transactions on Industry Applications*, vol. 53, no. 1, pp. 50–60, 2017.
10. S. Mezani, N. Takorabet, and B. Laporte, "A combined electromagnetic and thermal analysis of induction motors," *IEEE Transactions on Magnetics*, vol. 41, no. 5, pp. 1572–1575, 2005.
11. T. Voigdlener, D. Jochelavicius, and M. A. Peretti, "Thermal analysis of an induction motor by hybrid modeling of a thermal equivalent circuit and CFD," *IEEE Transactions on Industrial Electronics*, vol. 66, no. 3, pp. 2272–2280, 2019.
12. C. Ulu, O. Korman, and G. Kömürgöz, "Electromagnetic and thermal analysis/design of an induction motor for electric vehicles," *International Journal of Mechanical Engineering and Robotics Research*, vol. 7, no. 6, 2018.
13. M. Laïssaoui, M. R. Mékidèche, D. Sedira, and A. Ladjimi, "Dynamic modeling of induction motor taking into account thermal stresses," *COMPEL*, vol. 26, no. 1, pp. 139–150, 2007.
14. M. Iordache et al., "Dynamic performance analysis of deep bars squirrel cage induction motor by simulation," *Annals of the University of Craiova*, vol. 37, pp. 45–52, 2013.
15. P. D. Onwe, E. J. Akpama, O. I. Okoro, and O. Ekpenyong, "Dynamic behavior of asynchronous motor under balanced and unbalanced voltage source conditions," *World Journal of Engineering Research and Technology*, vol. 11, no. 4, pp. 239–252, 2025.

Corresponding author: Onwe Peter Daffin
peteronwe@unical.edu.ng
Department of Electrical and Electronic Engineering, University of Calabar, Nigeria.